SANDIA REPORT

SAND2013-8957
Unlimited Release
Printed October, 2013

Karst Characterization in a Semi-Arid Region using Gravity, Seismic, and Resistivity Geophysical Techniques

Kevin Scott Barnhart

Prepared by
Sandia National Laboratories
Albuquerque, New Mexico 87185 and Livermore, California 94550

Sandia National Laboratories is a multi-program laboratory managed and operated by Sandia Corporation, a wholly owned subsidiary of Lockheed Martin Corporation, for the U.S. Department of Energy's National Nuclear Security Administration under contract DE-AC04-94AL85000.

Approved for public release; further dissemination unlimited.

Sandia National Laboratories

Issued by Sandia National Laboratories, operated for the United States Department of Energy by Sandia Corporation.

NOTICE: This report was prepared as an account of work sponsored by an agency of the United States Government. Neither the United States Government, nor any agency thereof, nor any of their employees, nor any of their contractors, subcontractors, or their employees, make any warranty, express or implied, or assume any legal liability or responsibility for the accuracy, completeness, or usefulness of any information, apparatus, product, or process disclosed, or represent that its use would not infringe privately owned rights. Reference herein to any specific commercial product, process, or service by trade name, trademark, manufacturer, or otherwise, does not necessarily constitute or imply its endorsement, recommendation, or favoring by the United States Government, any agency thereof, or any of their contractors or subcontractors. The views and opinions expressed herein do not necessarily state or reflect those of the United States Government, any agency thereof, or any of their contractors.

Printed in the United States of America. This report has been reproduced directly from the best available copy.

Available to DOE and DOE contractors from
U.S. Department of Energy
Office of Scientific and Technical Information
P.O. Box 62
Oak Ridge, TN 37831

Telephone: (865) 576-8401
Facsimile: (865) 576-5728
E-Mail: reports@adonis.osti.gov
Online ordering: http://www.osti.gov/bridge

Available to the public from
U.S. Department of Commerce
National Technical Information Service
5285 Port Royal Rd
Springfield, VA 22161

Telephone: (800) 553-6847
Facsimile: (703) 605-6900
E-Mail: orders@ntis.fedworld.gov
Online ordering: http://www.ntis.gov/help/ordermethods.asp?loc=7-4-0#online

SAND2013-8957
Unlimited Release
Printed October, 2013

Karst Characterization in a Semi-Arid Region using Gravity, Seismic, and Resistivity Geophysical Techniques

Kevin S. Barnhart

Abstract

We proposed to customize emerging in situ geophysical monitoring technology to generate time-series data during sporadic rain events in a semi-arid region. Electrodes were to be connected to wireless "nodes" which can be left in the field for many months. Embedded software would then increase sampling frequency during periods of rainfall. We hypothesized that this contrast between no-volume flow in karst passageways during dry periods and partial- or saturated-volume flow during a rain event is detectable by these Wireless Sensor Network (WSN) geophysical nodes, we call this a Wireless Resistivity Network (WRN). The development of new methodologies to characterize semi-arid karst hydrology is intended to augment Sandia National Laboratorys mission to lead efforts in energy technologies, waste disposal and climate security by helping to identify safe and secure regions and those that are at risk. Development and initial field testing identified technological barriers to using WRNs for identifying semi-arid karst, exposing R&D which can be targeted in the future. Gravity, seismic, and resistivity surveys elucidated how each technique might effectively be used to characterize semi-arid karst. This research brings to light the importance and challenges with characterizing semi-arid karst through a multi-method geophysical study. As there have been very few studies with this emphasis, this study has expanded the body of practical experience needed to protect the nations water and energy security interests.

Acknowledgment

This work was funded under LDRD Project Number 157311 and Title "Hydrological Characterization of Karst Phenomenon in a Semi-Arid Region using In-situ Geophysical Technologies". Many thanks to Chuck Oden with Earth Science Systems LLC. The seismic portion could not have been accomplished without Nedra Bonal and Samantha Cafferky. Likewise, we are indebted to Jacob Sheehan and Zonge International for the conventional resistivity survey and results. Dennis Powers is responsible for geological consulting for the project, it was a great pleasure to learn from him. We would also like to thank Dirk O'Daniel, Michael Chapin, Wes DeYonge, Dale Bowman, for helping with the surveys. Michael Schuhen and Kris Kuhlman were unofficial mentors for this research.

Contents

1 Introduction . . . 9
2 Proposed Approach . . . 11
3 Methodologies and Results . . . 13
3.1 Field Site Selection . . . 13
3.2 Geological Model . . . 15
3.3 Gravity . . . 18
3.4 Seismic . . . 25
3.5 Wireless Resistivity Network . . . 26
3.6 Conventional Resistivity . . . 32
3.7 Other Low-Cost Ideas . . . 34
4 Conclusion . . . 40
References . . . 41

Appendix

A Additional 2D Gravity Results . . . 42

Figures

1 Cavernous openings in gypsum are less common examples of surface karst. The discarded refrigerator gives an idea of scale in the rightmost figure. These features are created by the dissolution of anhydrite layers. The dissolution of sulfate beds hundreds of meters below disturb the shallow geology by creating topological depressions and fractures to channel the water [3]. 9

2 A depiction of the various karst features that may form due to precipitation and how this water can be carried back to a central water source. 10

3 An aerial view of Dogtown. Sinkholes capable of channeling water to underlying karst are marked with green dots. Significant karstic depressions are marked in magenta. The yellow dot shows the approximate location of the S-06 corehole. The east to west line is evidence of a buried oil pipeline. The north to south line is an unmaintained caliche road. Those areas in dark grey are local valleys that support grass and creosote. The reddish areas are believed to be mudstone. 14

4 Stratigraphic drawings of the regional geology. Left, a general view of stratigraphic layers down to approximately 1400 meters. Note the location of the WIPP repository which is located NNW of the Dogtown site. The shallow geology of the Dogtown site resides in the Rustler formation, right, where outcroppings of the Forty Niner, Magenta, and Tamarisk members can be found within the surrounding alluvium. The sub-layers of the Rustler are labeled on the right. 16

5 A magnified portion of the geological map found in [1] of Dogtown. Magenta is denoted as 'Prm' and Forty Niner as 'Prf'. Where Bachman was unsure of the member of Rustler he simply labeled the area 'Pr'. There are two areas marked as 'Pdl', or Dewey Lake. The remainder is labeled to be either sandy or caliche alluvium, 'Qs' and 'Qa', respectively. Two sinkholes, 'SK', are identified. 17

6 Suspected geological cross-sections following the red lines in the upper image. Dashed green lines show the survey lines used for both gravity and seismic measurements. 'Qal' is alluvium, 'A-3' and 'A-4' are anhydrite layers which sandwich the Magenta dolomite, 'Mag', and 'M-4' is a mudstone. 19

7 S-06 (Shell Oil No. 6 or Dogtown No. 1 or U.S.G.S. No. 6) first 450 ft of gamma trace. The first 180 ft give an unusually high gamma signature when compared to other logs in the area. The Salado depth is reliably labeled at 425 ft BGS. 20

8 Survey location points for gravity survey. The line running SW to NE is called Line 1, and the line from SSW to NNW is called Line 2. The leftmost grid is called the GE grid, and the rightmost is called the Arroyo Grid. 21

9 Top, gravity data (minus baseline b-spline trend) in blue. Elevation is shown in yellow. The black points are gravity data with the elevation trend removed. Below, a linear trend is removed from the data which leaves anomalies. Two standard deviations from a student t-distribution are used on either side of the mean data point to construct the error bars in both figures. 23

10 Color maps of interpolated gravity data. Top left plot is raw data corrected only with baseline trend data; data follows topography closely. Top right plot shows the same data but with elevation effects removed; a strong planar trend is revealed. The bottom plot shows the data when a least-squared fitted planar trend is removed; gravity anomalies remain and are largely consistent with known and suspected areas of shallow karst (see Figure 3). 24
11 Seismic waves for 48-geophones for one source location of Line 1. In this figure, the P-wave is generally the first significant wave to reach the geophones. Two anomalies have been circled. In blue, the P-wave's amplitude is very small which may suggest interference of a void. In magenta, the P-wave seems to not arrive at all, suggesting a much larger interference in that direction. 25
12 Top, tomography results of the SW to NE line in Figure 8. Bottom, results of the SSW to NNW line. We hypothesize that the bottom of the Magenta formation is indicated near the light blue trend. Taking into consideration that the survey lines do not exactly coincide with the geological cross-sections (refer to Figure 6), we have taken the liberty of highlighting the areas of the geological cross-sections that correspond to the survey lines. The light blue undulations agree well with the base of the Magenta in the geological model, including the pinching out of the Magenta to the southwest of Line 1. This gives credence to the independently created geological model. 27
13 Top, seismic tomography results of 5-meter spaced grid measurements near arroyo, easternmost grid in Figure 8. Bottom, tomography results using a 2.5-meter spacing between measurement locations. The latter is clearly a better resolution for these karst features. 28
14 Left, a monitoring node in its polycarbonate housing. The antenna and solar cell are visible on the upper part of the unit. Top right, Schematic representation of a deployed node. Bottom right, Schematic of a resistivity survey. Current electrodes inject currents into the ground, and potential electrodes measure the resulting distribution of electric potential. 29
15 Left, a node implanted in the ground. Right, a cellular phone repeater providing internet access to the array of nodes. 30
16 Left, cellular telemetry system developed at Sandia National Laboratories in Carlsbad, NM. Top right, Digi Connectport X4 (CX4) cellular/wireless bridge device programmed with custom embedded python applications. Lower right, Decagon 5TE soil moisture sensor connected via RS-232 to serial port on the CX4. 31
17 Cores taken from outcroppings of the Magenta and Tamarisk formations, 2.2cm in diameter. Core slices, approximately half a centimeter thick, were used to estimate the resistivity of the two formations. 33
18 Measured log-scale resistivities of cores taken from Magenta and Tamarisk outcroppings. The two formations give distinctive resistivities, although both are highly resistive materials. 34
19 Location of resistivity probes shown red. The fourth line was skewed to the NNW because large mesquite bushes prevented the electrodes from being buried to the south. 35

20 Results of resistivity survey. All six lines were inverted independently and then results were interpolated to build this image. Large high-resistivity zone is located near suspected karstic areas, though we expected it to extend further to the north. X and Y are in latitudinal and longitudinal coordinates and depth is shown in feet. 36
21 A Desert Box Turtle, left, resting in a moist cow patty whose diet looks to have consisted of mesquite pods. Right, a Western Diamondback Rattlesnake, crossing the road. Rattlesnakes were often found at dawn near the two cavernous openings that seem to be connected according to the resistivity model. 36
22 Subsidence, dissolution, and erosion have sculpted an otherwise level landscape. Surface openings to karst porosity enables these processes to create arroyos, as pictured, which more quickly develop the topography and channel rain water. 37
23 Left, cavernous opening where a pressure transducer was staked with the purpose of detecting water runoff into the cave. Right, rain gauge installed on borehole marker from potash investigations in Section 3.2. 38
24 Results from pressure and rain experiment. Top shows the plot of the pressure gauge (given in psi) placed in the arroyo. Regional recorded barometric pressure (also given in psi) directly below. The difference between these two is given in the third row. There is nominal difference between the two, despite significant rain events (given in inches) shown in the final row. 38
25 Aerial photographs from 1996 and 2006, left to right, shown side-by-side to illustrate the dramatic difference in vegetation dependent upon seasonal rainfall. 39

1 Introduction

The dissolution of soluble bedrock, commonly limestone, results in surface and subterranean channels, caverns, and fractures, called karst, which comprises 7-10% of the dry earths surface. Karst may also form in other materials, such as the gypsum shown in Figure 1 where both shallow and deep geological process are both responsible.

Figure 1. Cavernous openings in gypsum are less common examples of surface karst. The discarded refrigerator gives an idea of scale in the rightmost figure. These features are created by the dissolution of anhydrite layers. The dissolution of sulfate beds hundreds of meters below disturb the shallow geology by creating topological depressions and fractures to channel the water [3].

Karst terrain has distinctive hydrology and landscapes which follow from a well-developed secondary porosity and high rock solubility, Figure 2. As a result, hydraulic conductivity is highly heterogeneous due to the interplay of dissolution, fracturing, diagenetic alteration and small-scale sedimentary structure. Such heterogeneity severely inhibits geological, geophysical and hydrological characterization.

Municipal, agricultural, energy, carbon storage, and waste projects are often projected for location in semi-arid regions where karst often exists but is extremely difficult to characterize using standard geophysical and hydrological methods. Karst can serve as a preferential conduit to focus surface and subsurface water but, because of irregular structure and nonlinear hydrodynamic behavior, is difficult to exploit as a water resource or protect from pollution. Hence, the scientific challenge exists to develop new techniques that gather karst hydrological information in terrains where karst features are dry except during infrequent rain and runoff events.

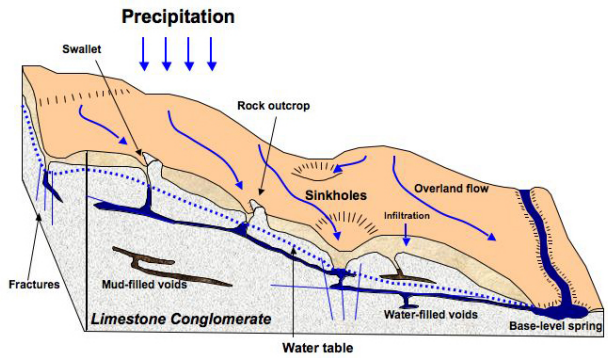

Figure 2. A depiction of the various karst features that may form due to precipitation and how this water can be carried back to a central water source.

Ground-based geophysical tools are typically chosen to locate karst structural features when water is limited or absent. Unfortunately, past field studies have met limited success because aforementioned subsurface heterogeneities confuse low-resolution data. Even when karstic conduits are located, the original questions, pertaining to conduit hydrological significance, are left unanswered. Previous karst hydrological studies mainly focus on wet karst systems in which discharge/recharge locations are known and persistent. In these areas, subsurface karst features may be inferred by analyzing water budgets, hydrographs or pumping tests. These methods assess the degree of karstification and the volume of groundwater resources in the saturated zone of the aquifer but cannot determine the structure of the karstic system. Further, they are substantially hindered in semi-arid climates.

Attempts to characterize commonly dry karst favor geophysical techniques – usually electrical and seismic methods. In such studies, karst phenomena are deduced from lower resistivities and seismic velocities than the surrounding rocks and also by strong lateral signal variations. However, even when ground-based geophysics are useful in localizing structural features (faults, fractures, altered areas, etc.) they are not commonly used to determine the position of saturated or unsaturated karstic conduits; nor do they infer to what degree these conduits are hydrologically significant. Recent studies to locate water using resistivity and seismic methods [4], advanced GPR technology [5] and magnetic resonance sounding equipment [7] have only seen application in non-arid climates.

Site characterization is a crucial step to locating suitable sites for weapon construction and storage, energy and carbon storage, waste disposal and other issues crucial to Sandia National Laboratories' safety and security missions. Through this research we seek a low-cost and versatile solution which may provide sufficient information to satisfy regulatory and safety requirements.

2 Proposed Approach

The proposed research is to utilize in situ geophysics devices to continuously monitor karst terrain over many months so that one can capture hydrological information on natures time scale in a semi-arid region. Thus, instead of merely detecting zones of enhanced dissolution, time-lapse data from before, during and after a rainstorm may reveal low-resistivity channels which transport water. State-of-the-art WSN technology, which combine low-power radio telemetry devices and energy harvesting methods, can be integrated with low-cost, low-power, in situ geophysical sensors to create geophysical WSN nodes. Embedded software could also be customized to listen to analog inputs of soil moisture content, rain gauge signals, or other natural excitations to determine resistivity sampling frequency. We intended to place these nodes near suspected karst recharge locations. The proposed resistivity technology can survey hundreds of meters radially and on the order of 100 meters in depth depending on the particular regional geology.

Water movement through the karst serves as a natural stimulus that is hypothesized to produce a signature of the event unique to each geophysical method. In contrast to traditional geophysical surveys, the effective subsurface properties are then transient responses resulting in a series of partial differential equations. Thus, time-dependent geophysical models and associated inverse methods will need to be developed to assimilate this data. For instance, the governing PDE for ohmic resistivity, assuming constant charge density, is found by $\nabla \cdot \mathbf{J} = 0$, $\mathbf{J} = -\sigma \cdot \nabla \mathbf{V} \Rightarrow \nabla\sigma \cdot \nabla \mathbf{V} + \sigma \nabla^2 \mathbf{V} = 0$; which relates the current density, $\mathbf{J}$, to the conductivity, σ, and potential, $\mathbf{V}$. Because of changing moisture content, conductivity is a function of time and now must be solved for multiple conductivity fields. These may be constructed by using Archies Law[1] and appropriate hydrological flow equations. This approach may be particularly useful for determining the mise-à-la-masse/2-D dipole-dipole survey design. Such models may be connected using multiphysics numerical software, such as Elmer, which plays a major role in both survey design and data analysis.

There are several challenges that contribute to the high-risk nature of this research. First is that in situ geophysics sensors and other WSN hardware are cutting-edge electronic equipment and, for this reason, may prove unreliable when left in harsh field conditions. Further, although these geophysics techniques have shown sensitivity to underground water, these in situ devices may lack the contrast needed to detect hydrologically significant karst conduit. Finally, like most karst geophysics studies to date, the inversion of field data may be difficult to constrain due to high model complexity and low data resolution, leading to a high degree of parameter uncertainty. We managed these technical risks to the best of our abilities and resources.

Various geophysical methods exist for investigating the subsurface, and most of them provide subsurface images of physical properties. Some geophysical imaging methods map areas where the subsurface rock properties change. In practice, sometimes a geophysical

[1] Archie's law is am empirical relationship between the in situ electric conductivity of a rock to its porosity and brine saturation. Though pervasive in hydrogeophysical studies, it remains difficult to predict parameter values, but no better alternative has found wide acceptance.

image of a subsurface property such as resistivity may be difficult to interpret because resistivity images may not always directly correlate with changing rock types. Geophysical surveys often produce repeatable data and images when no subsurface change occurs; but when change does occur, geophysical methods do a good job at detecting this change. For example, when subsurface fluid content changes, geophysical imaging is able to detect this change.

Change detection can be applied to the dolomites. The changing physical properties occur when rainwater from the seasonal monsoons flows through karst channels. Accordingly, an in-situ geophysical monitoring system should be able to observe the changing properties of the karst channels and thereby produce images of them. With this in mind, a wireless system for in-situ resistivity monitoring was created for a monitoring experiment in the semi-arid region of south-east New Mexico.

3 Methodologies and Results

Described below, is a high-level summary of the methods and results used in this project to characterize semi-arid karst. A field site was first selected according to a list of criteria. The local and surrounding geology is then discussed, and a conceptual geological model is provided. This model is a useful comparison when absorbing the results of the gravity, seismic, and resistivity surveys, whose descriptions are then provided. A Wireless Resistivity Network (WRN) section explains the development of the system and initial field trials and those results. Finally, descriptions of alternative low-cost ideas are given, which were pursued to varying degrees.

3.1 Field Site Selection

A field site was desired with the following criteria:

- Accessible location. Many trips to the site were anticipated with the need to possibly transport a variety of survey and monitoring equipment.
- Secure location to minimize the risk of theft or vandalism. Road signs and other "targets" near local rural roads often have bullet holes. Other signs of vandalism were a deterrent from picking a location which might endanger equipment.
- Possible flow in shallow karst during/after rain events. To realize change detection, we desired a location with low-lying openings with evidence of water flowing into subsurface channels.
- Access to karst recharge points for possible mise-à-la-masse survey technique. Additionally, we wanted to have the option of placing an electrode at the area of recharge to electrify the event of interest.
- A tame topography for easier modeling. It is often difficult to take into account dramatic landscapes into geophysical modeling analysis.

The site best chosen to meet these criteria is located 35 minutes, by road, SE of Carlsbad, NM. Borehole logging and other evidence indicated that this area was once referred to as "Dogtown", for unexplained reasons. This report refers to the study area roughly bounded by Figure 3 as "Dogtown", although it is unknown how much of the surrounding area was also once known by that name. The specifics of the site geology is explained in the proceeding section.

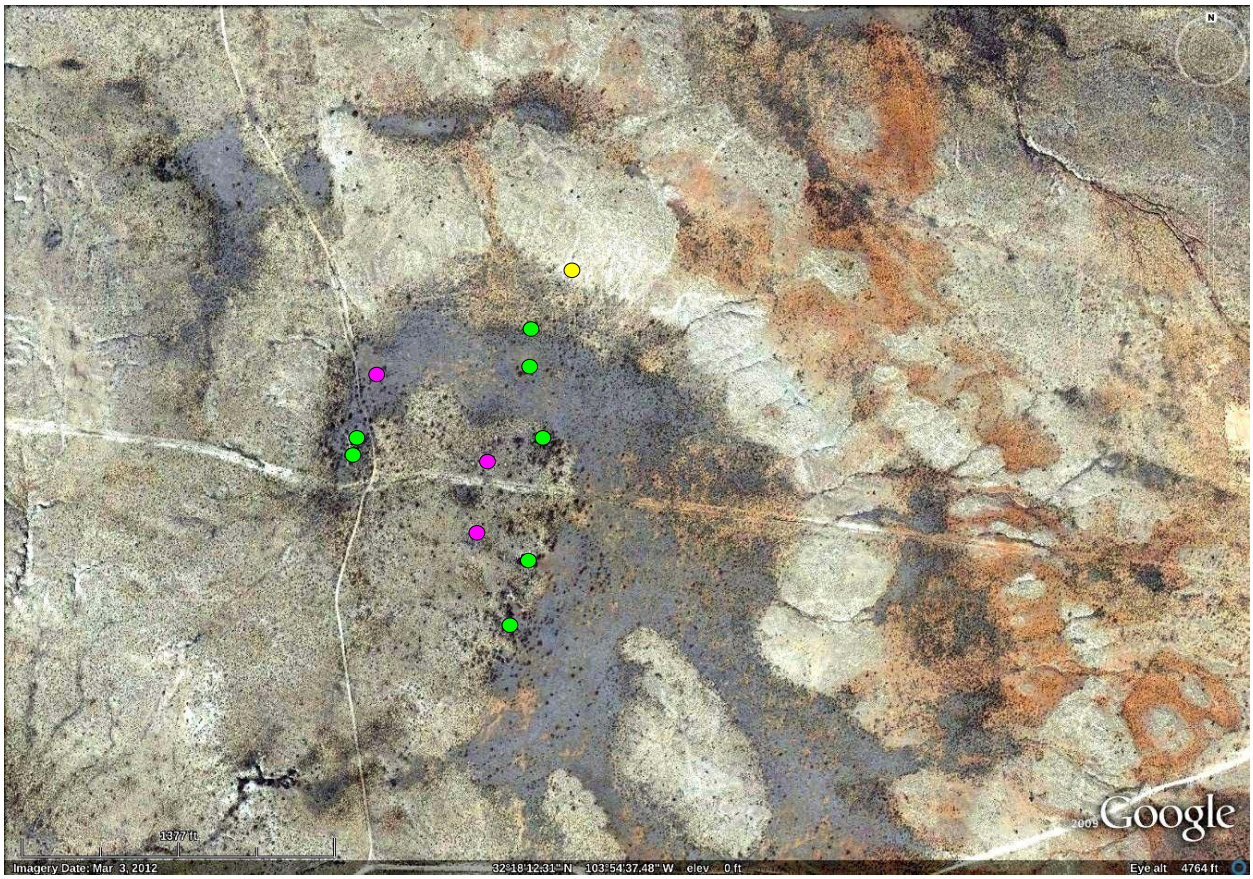

Figure 3. An aerial view of Dogtown. Sinkholes capable of channeling water to underlying karst are marked with green dots. Significant karstic depressions are marked in magenta. The yellow dot shows the approximate location of the S-06 corehole. The east to west line is evidence of a buried oil pipeline. The north to south line is an unmaintained caliche road. Those areas in dark grey are local valleys that support grass and creosote. The reddish areas are believed to be mudstone.

3.2 Geological Model

The local stratigraphy may be summarized and generalized by Figure 4. The Waste Isolation Pilot Plant is located 8.5 miles NE of the Dogtown Site in a bed of Halite. The stratigraphic members of interest to this shallow geophysical study all reside in the Rustler formation, where outcroppings of the Forty Niner, Magenta, and Tamarisk members can be found within the surrounding alluvium. Dogtown sits on the SE corner of a significant collapse of this stratigraphy, an area called Nash Draw. Nash Draw was created by the dissolution of the Salado formation, consisting primarily of salt, and to a somewhat lesser degree, the anhydrites located above the Salado by the ancestral Pecos river [1, 2, 6, 3]. Karstic terrain developed within the gypsum layers through both the dissolution of the anhydrites and also the breaking and shifting of the surface to accommodate the dissolution of the salts. This process continues today at a much slower pace as the Pecos river is a much smaller version of its former self and no longer passes through this area but to the West, near the towns of Carlsbad and Loving. Local potash refineries have contributed to the recent erosion processes through the often unintentional releasing of water from watering tailings piles.

Being near the edge of the geological feature, Dogtown is much less subsided than the lowest point of the draw, three miles to the NW. It sits on top of a hill, the draw dropping down more steeply to the north and to the west, and far more gradually to the south and east. A small, shallow hook-shaped valley captures rain from the surrounding ridges and channels them into low-lying valley areas – most of which have active sinkholes that collect the water. Just like the rest of the draw, the valley was likely created by salt and anhydrite dissolution, but to a lesser degree than most of Nash Draw, which provides clues about how Nash Draw may have been formed during the Paleolithic Age. Figure 5 from [1] outlines the topology and surface geology. There are many places where the Magenta is evident, denoted as 'Prm', and some Forty Niner, 'Prf'. Where Bachman was unsure of the member of Rustler he simply labeled the area 'Pr'. There are two areas marked as 'Pdl', or Dewey Lake, but closer inspection by Dennis Powers leaves us to believe that this is actually mudstone from the Forty Niner, or M4. The remainder is labeled to be either sandy or caliche alluvium, 'Qs' and 'Qa', respectively. Two sinkholes, 'SK', are identified, though we located several more as shown in Figure 3.

Figure 6 is Dennis Powers' interpretation of the shallow geology along two cross-sections, chosen to highlight the primary features of the area. The existence of M4 at the surface is unusual in the general area as it is easily eroded; its presence is indicative of how little rainfall this area has received. Powers suggests that the Magenta found towards the top of the ridge to the west is likely close to the original depositional elevation of the formation prior to the creation of Nash Draw. Note that the Magenta formation pinches off in near the inside of the valley's hook. It is precisely at these locations where most sinkholes are found, the water is seemingly cutting its way through the lower Magenta and upper Tamarisk and their interface. Other subsidences are noted near the top of the small hill enclosed by the hook and at various other locations in the valley, possibly evidence of where the Magenta is worn thin or is fractured and partially eroded. Lastly, we point out the severely disturbed

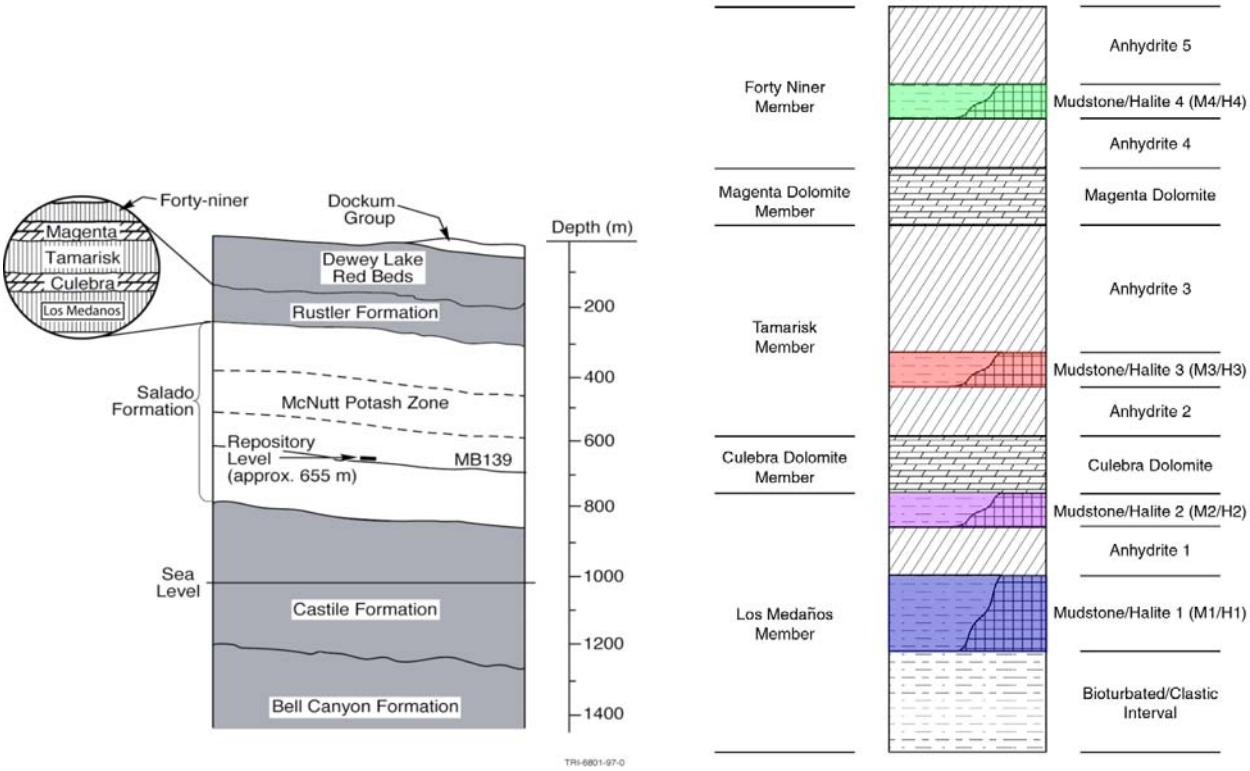

Figure 4. Stratigraphic drawings of the regional geology. Left, a general view of stratigraphic layers down to approximately 1400 meters. Note the location of the WIPP repository which is located NNW of the Dogtown site. The shallow geology of the Dogtown site resides in the Rustler formation, right, where outcroppings of the Forty Niner, Magenta, and Tamarisk members can be found within the surrounding alluvium. The sub-layers of the Rustler are labeled on the right.

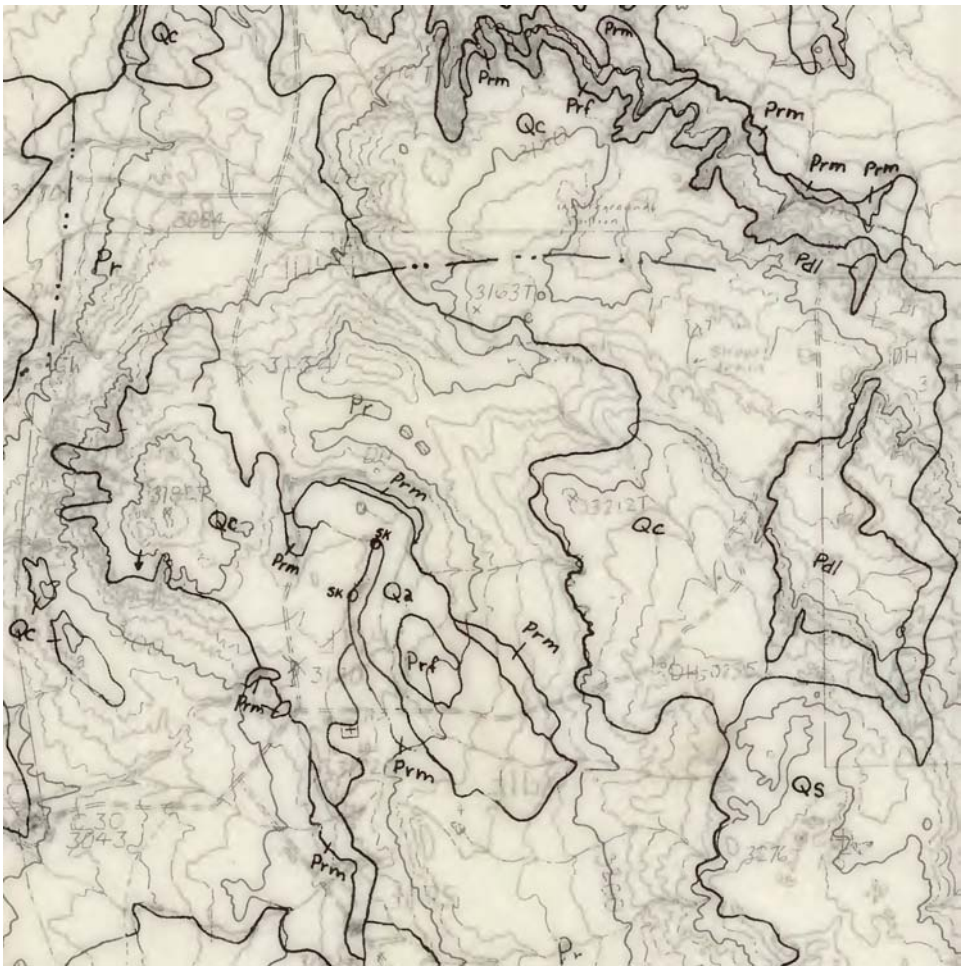

Figure 5. A magnified portion of the geological map found in [1] of Dogtown. Magenta is denoted as 'Prm' and Forty Niner as 'Prf'. Where Bachman was unsure of the member of Rustler he simply labeled the area 'Pr'. There are two areas marked as 'Pdl', or Dewey Lake. The remainder is labeled to be either sandy or caliche alluvium, 'Qs' and 'Qa', respectively. Two sinkholes, 'SK', are identified.

section of Magenta and Tamarisk in the SW region and note that other sinkholes exist in that area also.

Gamma Logs of Potash Corehole

An investigative potash borehole, or "core test", was drilled in January of 1963 by the Shell Oil Company at the Dogtown field site, seen in Figure 23 (right), in the NE side of the area of interest, see Figure 3. This was an attractive feature of the site; geophysical logs from the borehole investigation might be able to give stratigraphic picks on which to "hang" this study's geophysical interpretations. Not only was the Eddy County Bureau of Land Management (BLM) office able to provide the gamma and acoustic logs, but it appears that the logs were re-run at a slower speed with the primary goal of obtaining better shallow data (i.e., the first 500 ft). Figure 7 shows the results of the first 450 ft of the slower gamma log.[2] Unfortunately the acoustic velocity log wasn't run until after the Salado was reached.

We consulted local geology expert, Dennis Powers, who concurred that the shallow portion of this log is not very consistent with the general geology and with logs of nearby boreholes that he has analyzed. He suggested that the first approximately 250 ft of the log reflects fill that gives a clastic signature. After developing the geological model in Figure 6, it now seems likely that the high gamma signature is due to disturbed gypsum (probably Magenta) with other fill. One might conjecture that the re-logging of the shallow section of the borehole was done because no good interpretation was found on the first pass and the hope was that a higher resolution log would clear up the confusion.

3.3 Gravity

While concurrently working on the WRN, an opportunity presented itself to borrow an Autograv CG-5 gravimeter. Gravity surveys are not typically used to characterize karst because many data points are needed to obtain a good resolution (depending on the size of the feature to be located) and because it can take 5-10 minutes to collect data at each point. Because the gravitational field is highly correlated to elevation, it is also important to know a precise elevation at each measurement location, usually necessitating a professional GPS survey which can also be time-consuming. Nevertheless, we rented GPS surveying equipment and obtained precise elevation, within 2cm, and latitudinal and longitudinal coordinates for: (i) a 96-point line running SW to NE, called Line 1; (ii) a 92-point line running SSW to NNW, called Line 2; (iii) a western 44-point grid over an area with many sinkholes, called GE Grid due to the old refrigerator in one of the sinkholes (see Figure 1); (iv) and an eastern 49-point grid located around a karstic arroyo (see Figure 22), called Arroyo Grid. The survey locations are shown in Figure 8. The idea was to get a general picture of the local area with the two lines and obtained finer detail around known karstic regions using the grids.

[2]The rest of the log is not shown because it is not relevant to this project, and also because it may provide corporate-sensitive knowledge of the location of potash layers.

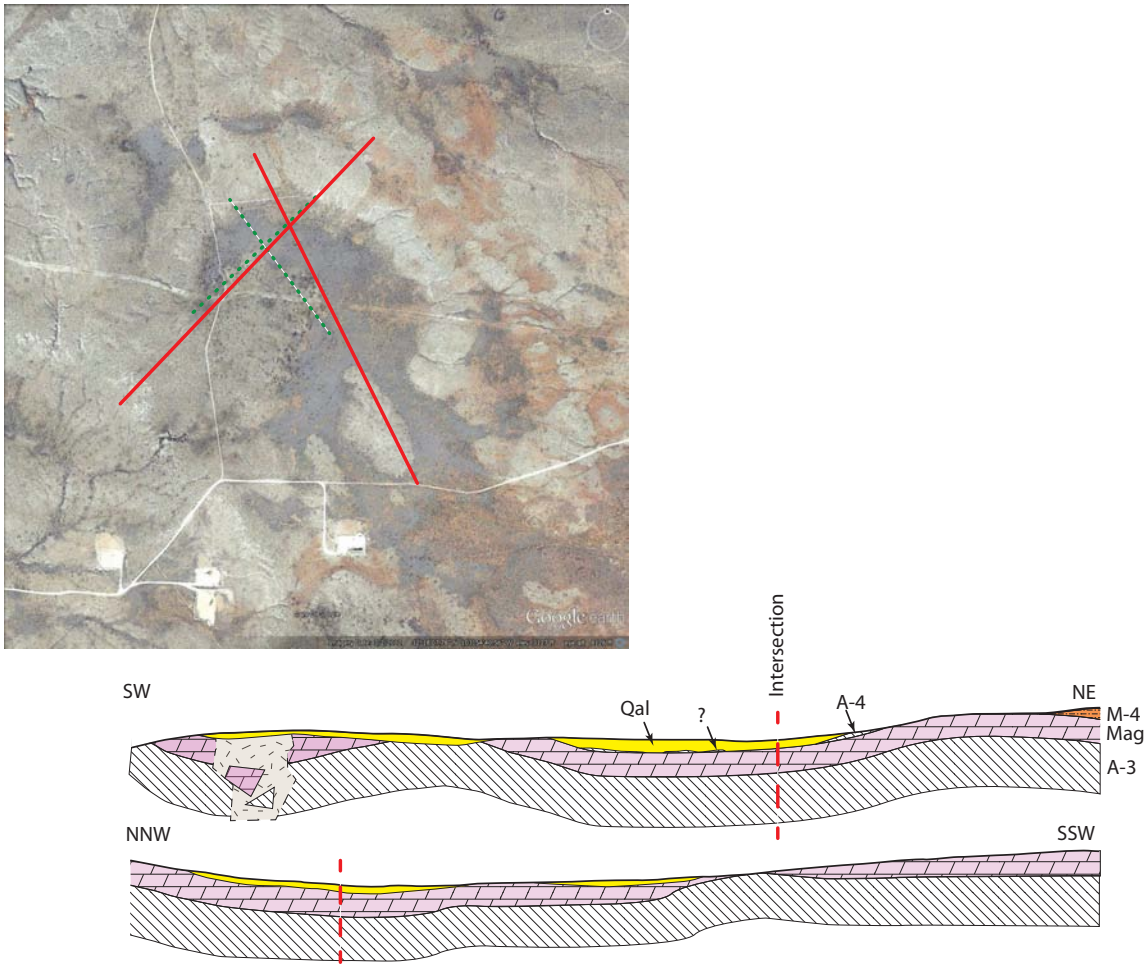

Figure 6. Suspected geological cross-sections following the red lines in the upper image. Dashed green lines show the survey lines used for both gravity and seismic measurements. 'Qal' is alluvium, 'A-3' and 'A-4' are anhydrite layers which sandwich the Magenta dolomite, 'Mag', and 'M-4' is a mudstone.

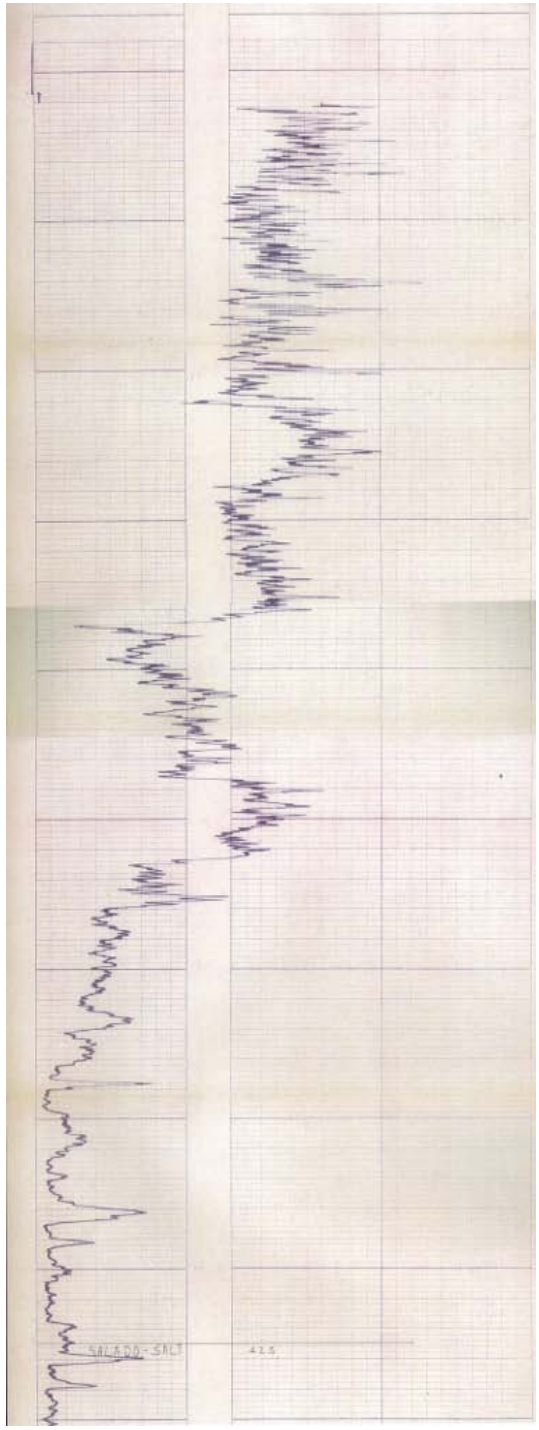

Figure 7. S-06 (Shell Oil No. 6 or Dogtown No. 1 or U.S.G.S. No. 6) first 450 ft of gamma trace. The first 180 ft give an unusually high gamma signature when compared to other logs in the area. The Salado depth is reliably labeled at 425 ft BGS.

Figure 8. Survey location points for gravity survey. The line running SW to NE is called Line 1, and the line from SSW to NNW is called Line 2. The leftmost grid is called the GE grid, and the rightmost is called the Arroyo Grid.

The Autograv CG-5 gravimeter measures acceleration in Milli-gal (Mgal)[3] relative to a known datum. The instrument calculates acceleration by measuring how much an internal spring is stretched by a weight. Wind or other disturbances and changes in temperature can all effect the accuracy because of this configuration. We selected a central base point location at which we re-measured the gravity every hour while conducting the survey. By creating a b-splined time-series, baseline, we were able to correct for drift and environmental conditions throughout the day. Additionally, the unit was configured to take five samples for each location, each sample consisting of an average of over 20 internal readings. The variability of the samples can be seen immediately after conducting the measurement, and we re-measured more than a dozen locations because they did not initially meet our data quality criteria. Multiple readings at each location can also provide a quantitative measure of accuracy using a student t-distribution to calculate confidence intervals; these are displayed for each data point in the figures.

Figure 9 shows the data for Line 2 with baseline correction applied. The upper plot visually shows the correlation of the elevation to the data and what the data looks like after correction. After removing a least-squared fitted elevation trend[4], a strong linear trend was seen in the remaining data. We hypothesize that this linear trend (planar in 3-dimensions as shown in Figure 10) is due to the slope of the Tamarisk formation in the immediate region; as this site is near the edge of Nash Draw, some stratigraphic layers are sloped towards the draw due to large scale Salado dissolution. Removing this linear trend leaves gravity anomalies which may indicate karst or some other change in density.

Gravity line plots and their corrections for Line 1 and the two grids can be found in Appendix A. We applied the baseline and elevation corrections to all of the data simultaneously, see Figure 10. This result was a planar trend consistent with our sloping Tamarisk hypothesis. A useful aerial view of the anomalous gravity data is also given in Figure 10, created by removing a planar trend from the data, fitted using least-squares, and then interpolating the data over a regular grid. This color plot shows areas of low gravity surrounding areas with visible surface karst and karst-like features. It may be useful to compare this with Figure 3. With some confidence in a geological model, these results suggest that gravity may be a viable indicator of karst. However, in areas where subsurface density is naturally heterogeneous due to other features, analysis could be especially inconclusive. To also note, the analysis of gravity data cannot typically distinguish between a wide, shallow feature and a narrow, deep feature, which is another reason that gravity results alone may not give sufficient characterization.

[3]One gal is defined as one centimeter per second squared.

[4]Elevation is not typically removed from gravity data in this way. The usual manner is to perform a Bouguer correction which is the removal of a linear elevation trend given an estimated density of the earth. As we were more interested in finding anomalies in the gravity data than in developing an accurate model, we remove the largest linear elevation trend possible.

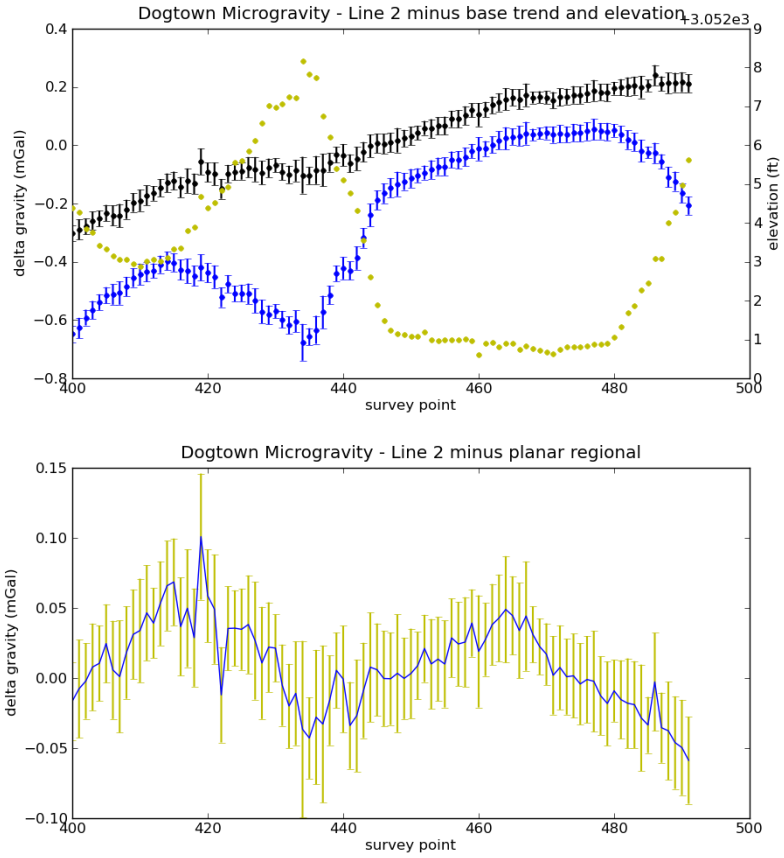

Figure 9. Top, gravity data (minus baseline b-spline trend) in blue. Elevation is shown in yellow. The black points are gravity data with the elevation trend removed. Below, a linear trend is removed from the data which leaves anomalies. Two standard deviations from a student t-distribution are used on either side of the mean data point to construct the error bars in both figures.

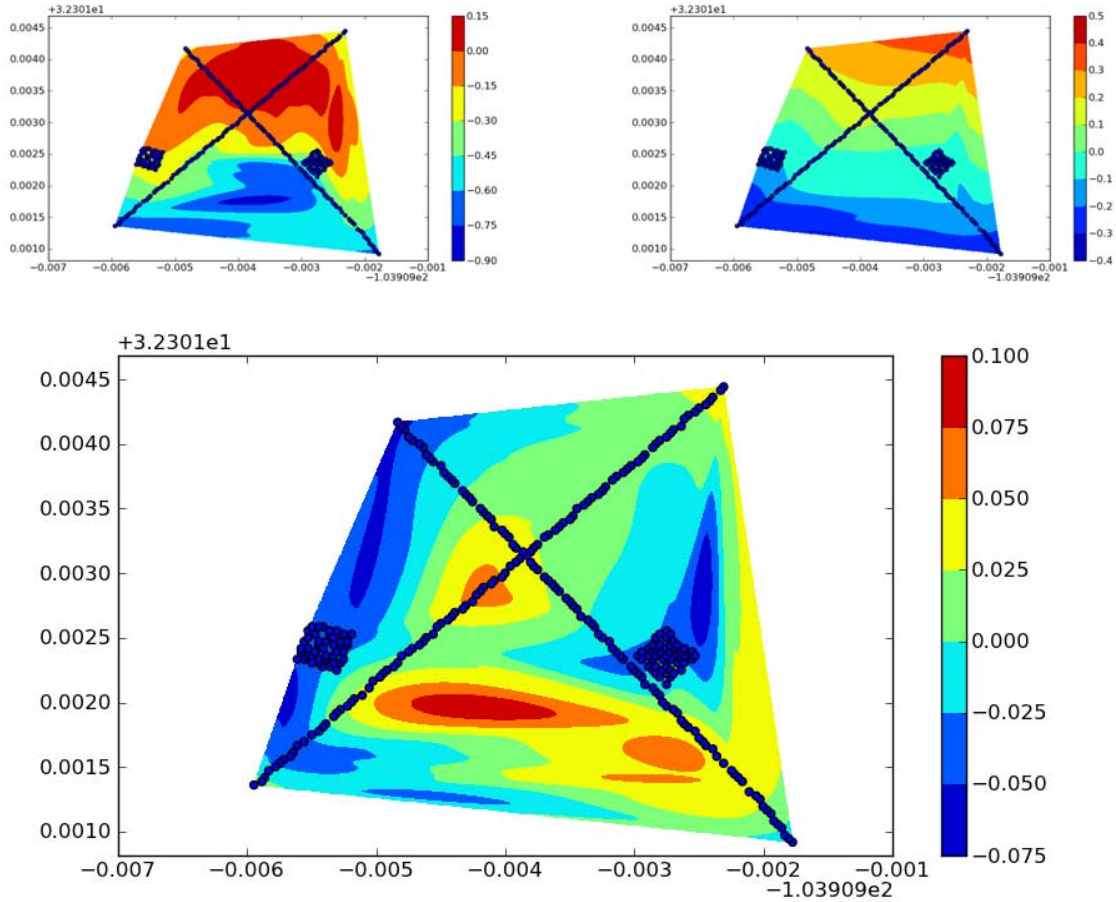

Figure 10. Color maps of interpolated gravity data. Top left plot is raw data corrected only with baseline trend data; data follows topography closely. Top right plot shows the same data but with elevation effects removed; a strong planar trend is revealed. The bottom plot shows the data when a least-squared fitted planar trend is removed; gravity anomalies remain and are largely consistent with known and suspected areas of shallow karst (see Figure 3).

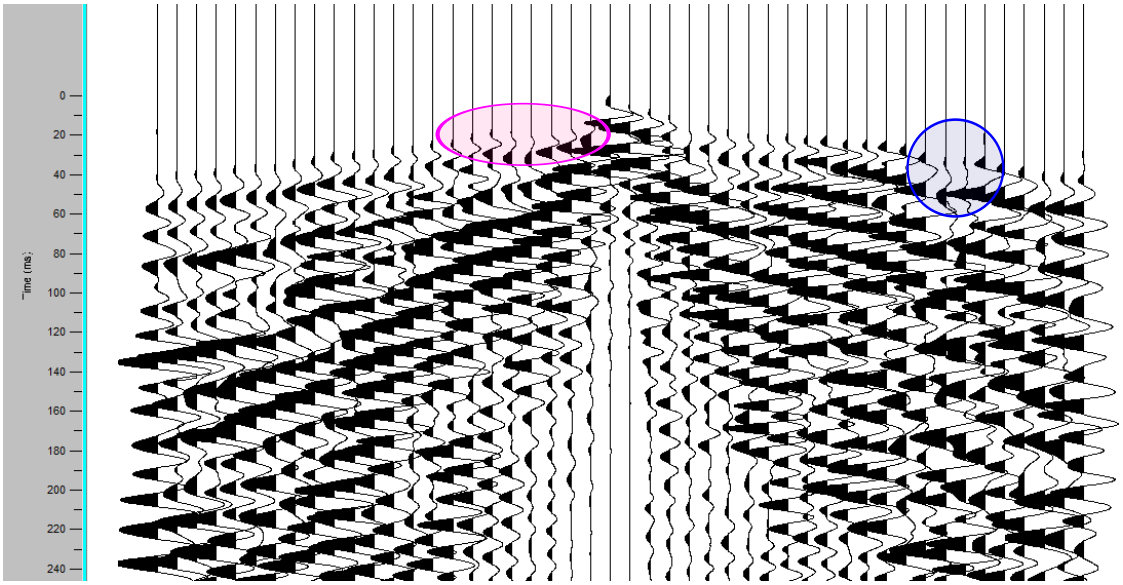

Figure 11. Seismic waves for 48-geophones for one source location of Line 1. In this figure, the P-wave is generally the first significant wave to reach the geophones. Two anomalies have been circled. In blue, the P-wave's amplitude is very small which may suggest interference of a void. In magenta, the P-wave seems to not arrive at all, suggesting a much larger interference in that direction.

3.4 Seismic

A refractive seismic survey was conducted over Line 1 and 2 of the gravity survey, shown in Figure 8. Seismic data was also gathered over the same Arroyo grid, which has 5-meter spacing between points, as the gravity survey. Additionally, two 2.5-meter spaced grids were laid out over the original Arroyo grid to obtain additional resolution. The seismic phenomenon was produced by impacting a sledge hammer on a metal plate in between each data point. This sounding was measured by geophones and acquired by two 24-channel GEODE data acquisition systems manufactured by Geometrics. Multiple hits of the hammer were used to "stack" the measurements which effectively amplifies the signal while adding out noise. The raw data output of one source location and the measured response of 48 geophones is shown in Figure 11. We then hand-selected the arrival time of the P-wave at all geophones for all source locations over both lines and both grids, a very time-consuming task.[5] We used Seismic Processing Workshop (SPW) by Parallel Geosciences, Matlab by the Mathworks, and Sandia's in-house tomography inversion code to process the data.

[5]There are automatic picking tools available, but these are only useful for a very regular subsurface. However, such tools can sometimes be useful for providing a good first guess, but manual inspection is often still necessary.

Several features were seen in the raw data that may indicate karstic voids: slow P-wave arrivals, polarity reversals, and decreased P-wave amplitudes, seen in Figure 11. One method of stitching the raw data together is by inverting the subsurface model with a tomography code. The results of Sandia's tomography code on Line 1 and 2 data is shown in Figure 12. The results are explained fully in the caption of the figure where the geological cross-sections from Figure 6 have been included for comparison. Example plots for the 5-meter and 2.5-meter spaced grids are shown in Figure 13. The results of the 5-meter spaced grid are relatively uniform and inconclusive, showing no evidence of voids or some other stratigraphic disturbance. In contrast, the 2.5-meter grid gives far better resolution.

3.5 Wireless Resistivity Network

Figure 14 depicts a sensor node that was designed to be permanently installed in the field so that periodic sensor readings could be made. The sensor contains a wireless radio for telemetry, a solar cell to recharge internal batteries, and circuitry for making subsurface resistivity measurements. The resistivity circuitry includes a high voltage power supply for injecting survey current into the ground, and an array of precision voltmeters for measuring the resulting electrical potentials (see Figure 14). Each node supports an array of eight electrodes that can function as current injection electrodes of potential measuring electrodes. The nodes were designed to be partially buried as shown in Figure 14, and the electrodes and connecting wires are entirely buried. An entire area can be monitored with an array of nodes, and successively injecting current in many different locations and monitoring the resulting potentials can generate an image of the subsurface.

A set of 25 nodes was built for monitoring the shallow karst at the Dogtown site. A photo of an installed node is shown in Figure 15. A cellular data link (or repeater) provided a communications bridge between the internet and the sensor nodes (see Figure 15). This particular cellular repeater solution relayed commands and forwarded data from a network of test nodes in the field. This design required constant cellular connectivity from the lab, where a computer was running the commanding Python scripts and the cellular repeater. Occasional cellular outages due to low signal strength and timing issues due to communication delays threatened the reliability of this approach.

In response to the difficulties with the initial cellular repeater, we built a cellular repeater station, seen in Figure 16 which used a cellular repeater device manufactured by Digi International Incorporated which runs an embedded Python interpreter. We were able to secure shell into this cellular repeater from the lab and program the Digi Connectport X4 (CX4) to run a set of Python scripts upon reboot. Rebooting the device, uploading new scripts, and checking device status was simply performed using Digi's online Device Cloud website. Additionally, we programmed the 9-pin serial port on the CX4 to communicate with a Decagon 5TE soil moisture probe, also in Figure 16, so that the network management Python scripts could automatically adjust to changing conditions. The CX4 platform was not without limitations, however, and we would suggest that a repeater be used that is running an embedded Linux OS for more flexibility.

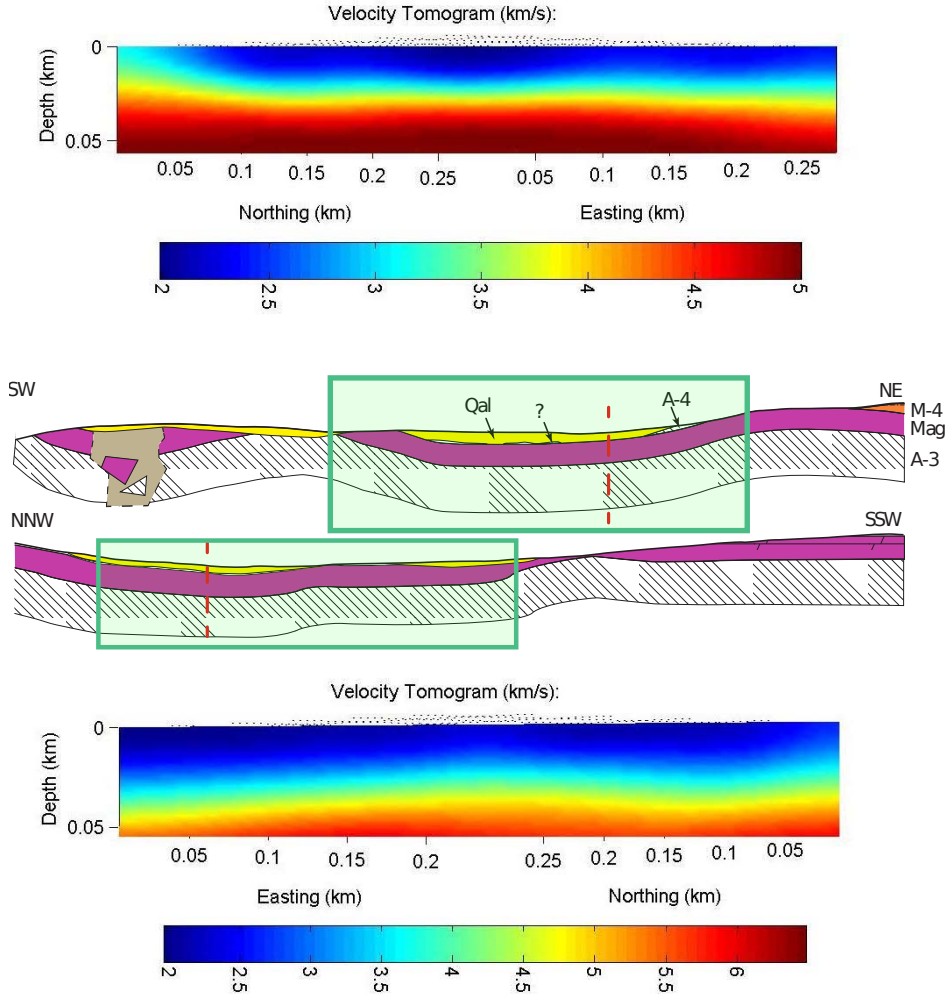

Figure 12. Top, tomography results of the SW to NE line in Figure 8. Bottom, results of the SSW to NNW line. We hypothesize that the bottom of the Magenta formation is indicated near the light blue trend. Taking into consideration that the survey lines do not exactly coincide with the geological cross-sections (refer to Figure 6), we have taken the liberty of highlighting the areas of the geological cross-sections that correspond to the survey lines. The light blue undulations agree well with the base of the Magenta in the geological model, including the pinching out of the Magenta to the southwest of Line 1. This gives credence to the independently created geological model.

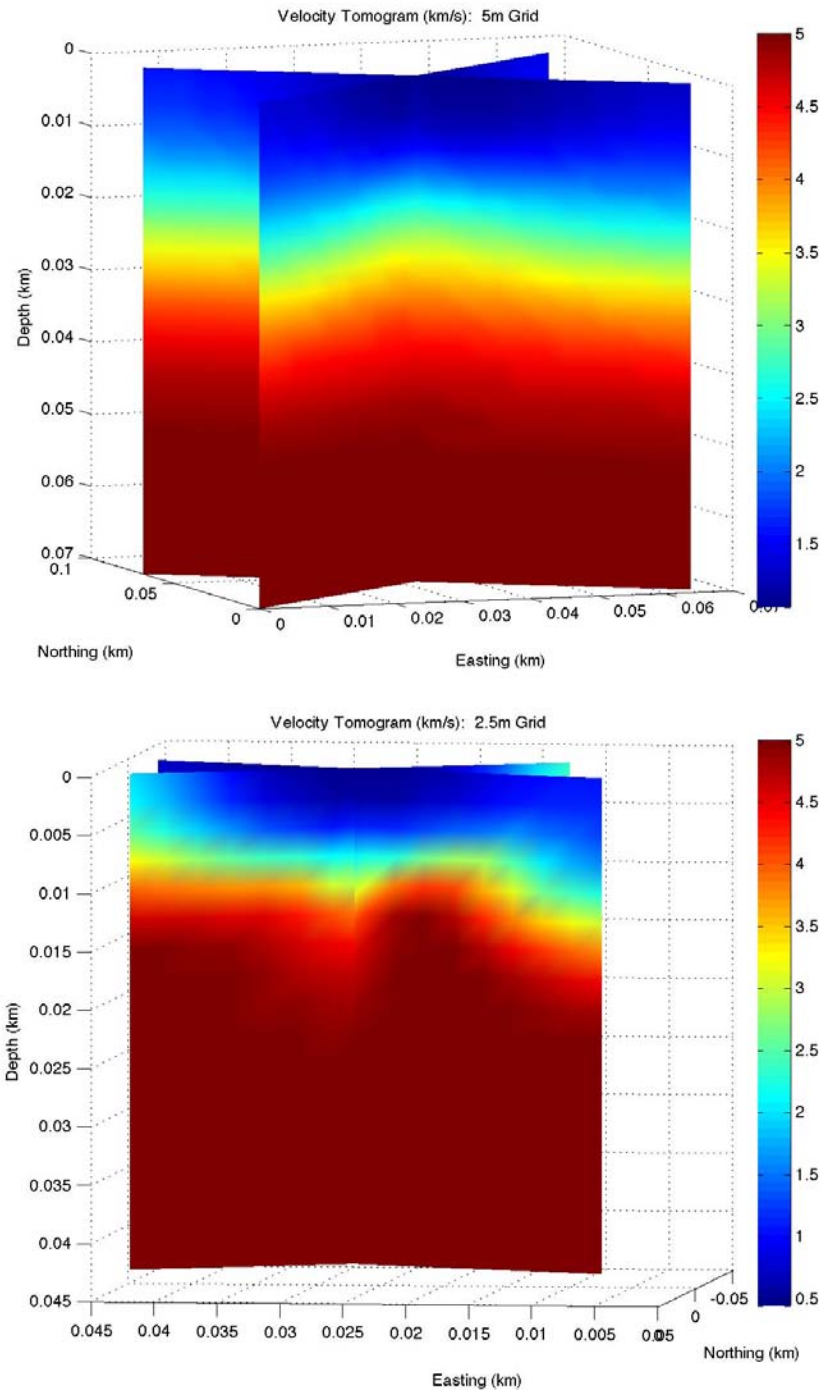

Figure 13. Top, seismic tomography results of 5-meter spaced grid measurements near arroyo, easternmost grid in Figure 8. Bottom, tomography results using a 2.5-meter spacing between measurement locations. The latter is clearly a better resolution for these karst features.

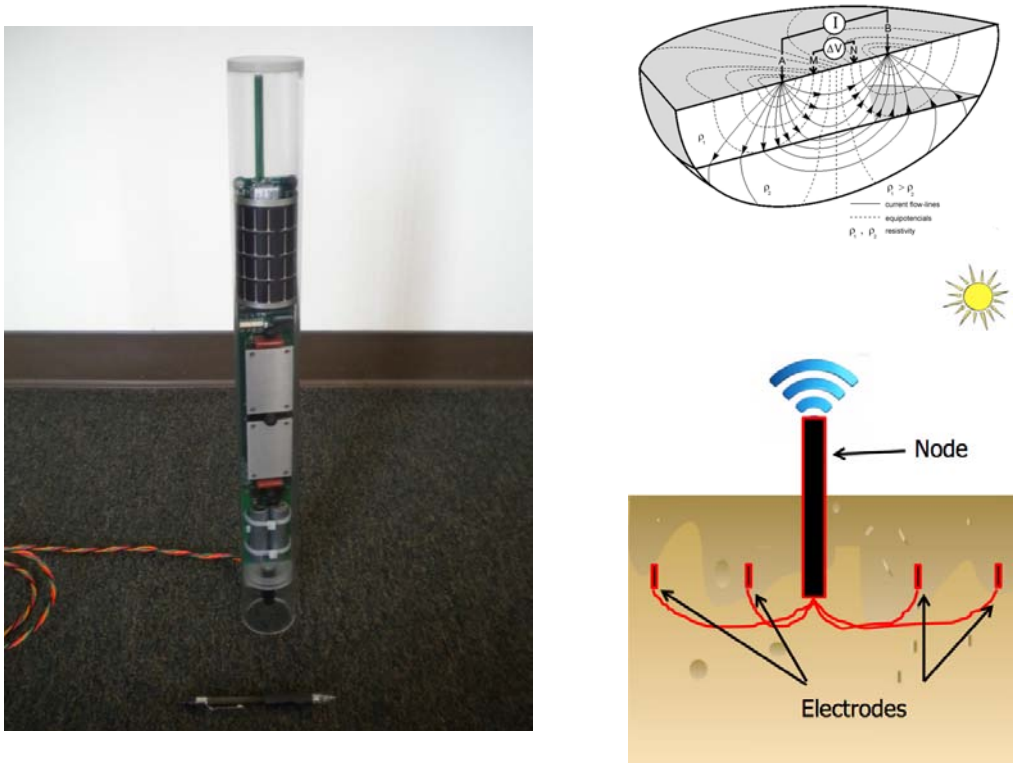

Figure 14. Left, a monitoring node in its polycarbonate housing. The antenna and solar cell are visible on the upper part of the unit. Top right, Schematic representation of a deployed node. Bottom right, Schematic of a resistivity survey. Current electrodes inject currents into the ground, and potential electrodes measure the resulting distribution of electric potential.

Figure 15. Left, a node implanted in the ground. Right, a cellular phone repeater providing internet access to the array of nodes.

Aside from the cellular repeater challenges, after the nodes were installed they did not perform as anticipated. Several shortcomings were identified with the system; and this project did not have sufficient time or budget to see solutions to the difficulties. We believe that the monitoring node concept is viable, but more development is needed before the technology is ready for routine monitoring applications.

The housings were made from 3/16 inch walled polycarbonate tubing. Polycarbonate has good impact resistance and is used to make bullet resistant windowpanes. However, our testing showed that they would not withstand bullet impacts and likely not hail stone impacts both of which are issues in the American West. We recommend that future nodes should be encased in steel housings.

The biggest difficulty was the node's power systems. The voltmeters and radio are low power devices with a low duty cycle that can easily be supported by a small solar recharged battery system operating from a single 3.6 VDC LiPO4 cell. The LiPO4 battery chemistry was chosen because it offered more charge/discharge cycles (i.e. longevity) than other chemistries and it also has good energy density. The current injection electronics is a high power system, and supporting such a system from a small solar cell proved more challenging. The high power system operated on a 14.4 VDC battery system (four 3.6 V cells), and the solar cell output voltage (nominally 4-5 VDC depending on solar intensity) had to be stepped up to charge the 14.4 V batteries. Furthermore, the charge state of each cell needed to be separately monitored to prevent over charging or over depletion. This was not done properly. Finally, after conducting winter experiments we found that there is no battery chemistry that can be charged in freezing conditions. Several improvements were made during this project, but complete improvements addressing all of these issues were not completed. There were also battery difficulties with the repeaters (see Figures 15 and

Figure 16. Left, cellular telemetry system developed at Sandia National Laboratories in Carlsbad, NM. Top right, Digi Connectport X4 (CX4) cellular/wireless bridge device programmed with custom embedded python applications. Lower right, Decagon 5TE soil moisture sensor connected via RS-232 to serial port on the CX4.

16). The repeaters used sealed lead-acid batteries, which did not initially operate properly in a cold weather test; this issue was mitigated by replacing the batteries with deep-cycle batteries, though no batteries charge well in cold temperatures. For future monitoring nodes, we recommend replacing batteries with super capacitors. Although super capacitors are more bulker and more difficult to interface to the electronics, they do not have the temperature limitations and charge monitoring requirements.

The final difficulty was with the node array management server. This server's function was to schedule surveys, manage the sleep and wake schedules of the nodes and the repeater, configure the nodes for different survey operations, and orchestrate the surveys. The chief difficulty here was that the software scripts were too complex to be setup and administered by non-developers, and setting up a resistivity survey sequence with many electrode configurations was daunting. Until the survey software is further developed, we recommend that the system developers conduct the survey configuration, administration, and operation.

Many areas for future research came out of this investigation, despite the failure of this project to prove the function of a WRN for monitoring change detection in shallow karst.

3.6 Conventional Resistivity

We conducted a low-cost, conventional DC resistivity survey with the support of Zonge International at Dogtown in lieu of the planned WRN survey. We felt that it was important to evaluate the effectiveness of the resistivity technique even without teasing out additional resolution using change detection.

We sought to determine the resistivity of the alluvium in which the resistivity probes would be placed. This is an important parameter for survey design since it is imperative that sufficient current be able to pass in between nodes for measurement. Overcoming contact resistance, the resistance at the contact between the probe and soil, is usually the biggest factor. A Digital Insulation Tester Meter Megger Megohmmeter VC60 was used to measure resistance between electrodes and we obtained resistances in the 10's of kΩ by simply burying the electrodes in the soil. Resistances of 4,000-8,000 kΩ were achieved during the actual survey after burying the nodes in a hole packed with wet bentonite to reduce the contact resistance.

After determining that soil resistance was reasonable, 2.2cm diameter cores were removed from the Magenta and Tamarisk outcroppings to determine if their conductances were sufficiently dissimilar to distinguish them in analysis. The cores were sliced using a rock saw with a diamond-encrusted cutting wire to an approximate thickness of 0.5cm. Both cores and slices are shown in Figure 17. Both surfaces of each slice were coated in a conductive paint in order to uniformly distribute current. Surface area of each slice was estimated by scanning in images of the slices into a computer software which could calculate the area of a traced shape. A digital fractional caliper was used to estimate the thickness of each slice. Assuming each slice is uniform in its cross section, the resistivity in units of ohm meters is

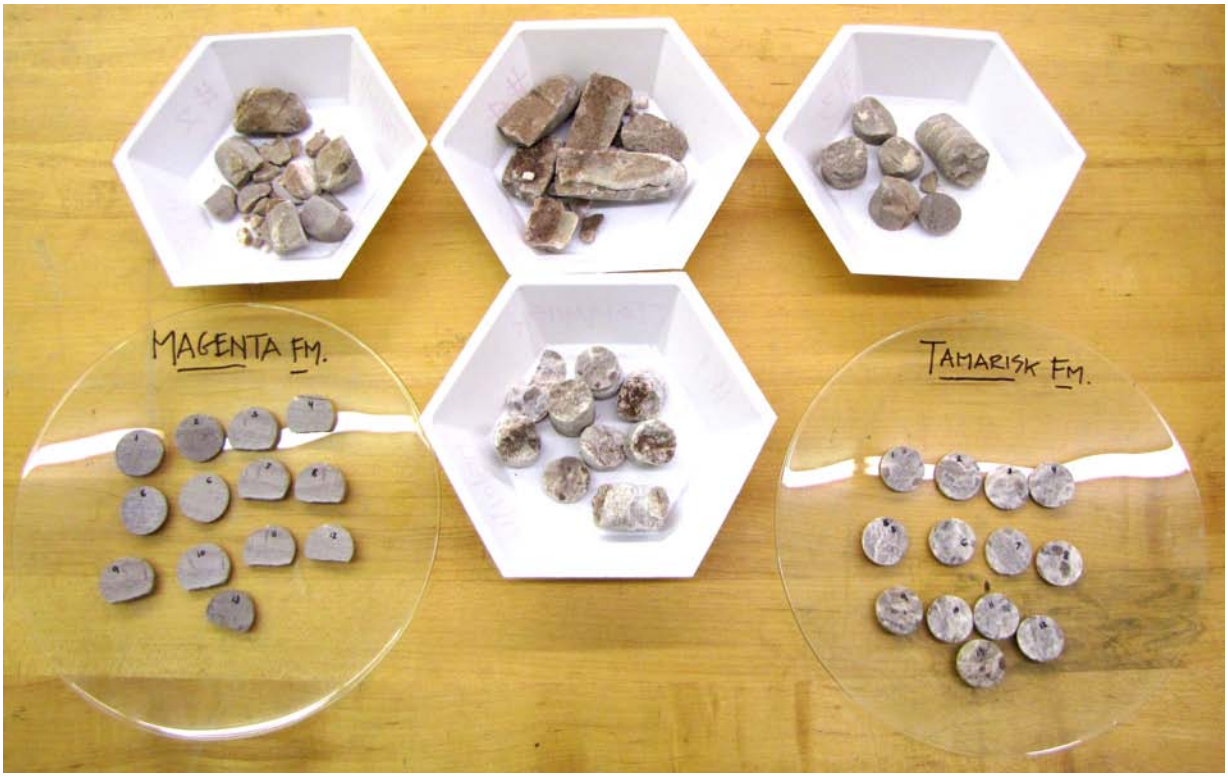

Figure 17. Cores taken from outcroppings of the Magenta and Tamarisk formations, 2.2cm in diameter. Core slices, approximately half a centimeter thick, were used to estimate the resistivity of the two formations.

given by: $\rho = R * SA/l$, where R is the resistance in ohms, SA is surface area in meters, and l is the length of the sample in meters. The results are shown in Figure 18. Although the magnitude of the final results may be different by an order of magnitude or more in the field, due to the existence of conductive paths, these results are important since they show that the two formations have distinctive resistances.

Mimicking the intended WRN installation, six lines of electrodes were located near the Arroyo grid and continuing into the local valley, refer to Figure 19. Each line contained 24 12" stainless steel electrodes as if 3 wireless resistivity nodes were used to command 8 electrodes on each line. The survey was designed to help determine the location of any low resistivity zones and perhaps to understand the extent to which the Magenta pinches off into the valley (return to Figure 6).

A rain from five days earlier left residual soil moisture enabling good connectivity between electrodes. Each line was measured independently. A resistivity model was created for each line by inverting the data using Zonge's software, also independently of each other. All models were combined and spaces in between the lines interpolated to generate Figure

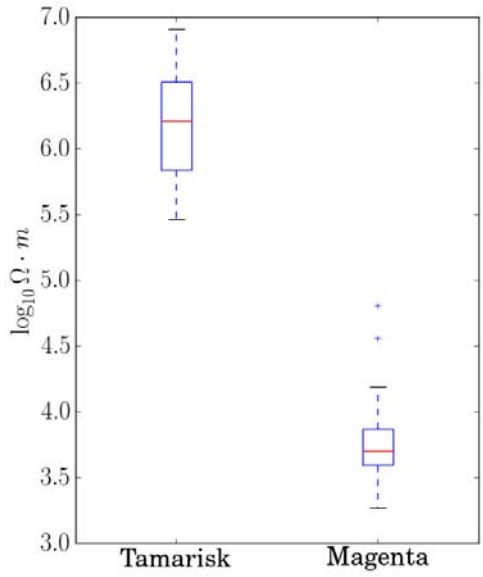

Figure 18. Measured log-scale resistivities of cores taken from Magenta and Tamarisk outcroppings. The two formations give distinctive resistivities, although both are highly resistive materials.

20. The results show an especially high resistivity area near the cavernous openings and extending well into the valley and towards sinkholes and depressions near the center of the valley, reference Figure 3. The modeled high-resistance feature is large enough to suggest possible hydrological connectivity, and certainly a good habitat for desert-dwelling animals such as the Desert Box Turtle and Western Diamondback Rattlesnake in Figure 21, both photographed at the Dogtown location.

3.7 Other Low-Cost Ideas

The existence and location of hydrologically connected, semi-arid karst might be inferred from other low-cost techniques which might be overlooked. We considered and experimented with a few of these in this study but suggest further studies in order to understand their capabilities.

Rain and Pressure

In the vein of low-cost semi-arid karst characterization solutions, a 0-30psi pressure transducer gauge with internal datalogger was staked to the surface of the ground at the bottom of a low-lying arroyo, see Figures 22 and 23. A rain gauge was installed on an old potash corehole marker, Section 3.2, to record rainfall. It was hypothesized that sufficient runoff

Figure 19. Location of resistivity probes shown red. The fourth line was skewed to the NNW because large mesquite bushes prevented the electrodes from being buried to the south.

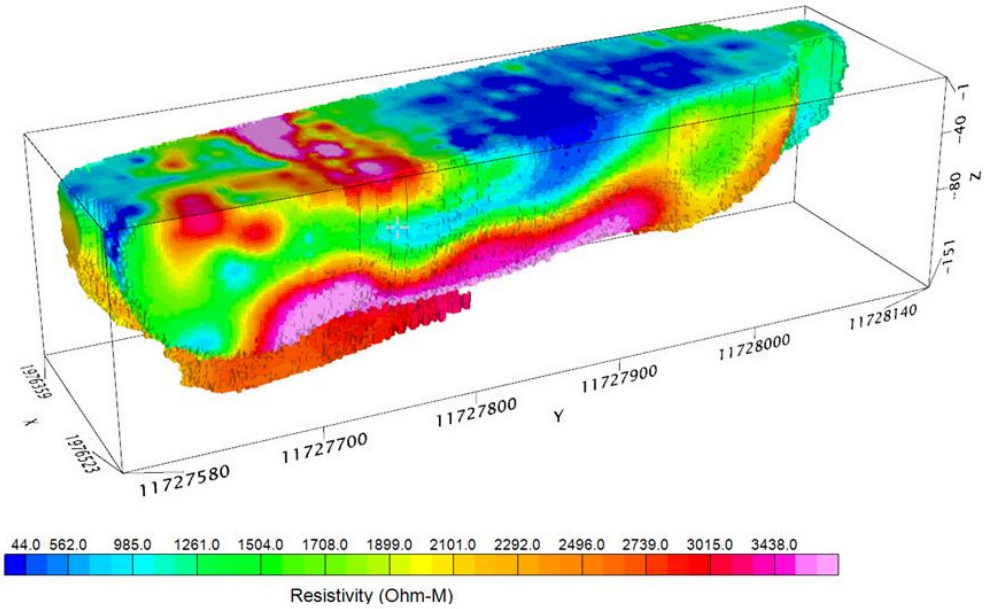

Figure 20. Results of resistivity survey. All six lines were inverted independently and then results were interpolated to build this image. Large high-resistivity zone is located near suspected karstic areas, though we expected it to extend further to the north. X and Y are in latitudinal and longitudinal coordinates and depth is shown in feet.

Figure 21. A Desert Box Turtle, left, resting in a moist cow patty whose diet looks to have consisted of mesquite pods. Right, a Western Diamondback Rattlesnake, crossing the road. Rattlesnakes were often found at dawn near the two cavernous openings that seem to be connected according to the resistivity model.

Figure 22. Subsidence, dissolution, and erosion have sculpted an otherwise level landscape. Surface openings to karst porosity enables these processes to create arroyos, as pictured, which more quickly develop the topography and channel rain water.

into the arroyo would be visible in the transducer data and this would correlate to the rainfall data given by the rain gauge. As shown in Figure 24, either runoff was insufficient or transducer placement was poor (or both) to provide meaningful results.

Vegetation study

Consider the images in Figure 25. The left aerial photo is of Dogtown in 1996 after a significant drought. In contrast, the right aerial photo shows the site after the monsoon season in 2006. The types and location of vegetation during dry and wet periods can provide clues as to where water is located in different conditions. At this site, unusually large mesquite bushes seem to be a reasonable predictor of shallow karstic water resources during periods when water may not be available to other vegetation. An in depth study might include some excavation to determine root depths and detailed photo analysis. This approach may be prove to be particularly useful for areas with shallow karst. Further, it would be largely unobtrusive and may scale inexpensively to include larger areas.

Acoustic monitoring at recharge locations

Future research may consider placing a low-frequency acoustic recording device near a karst recharge location, such as the top picture if Figure 23. Careful analysis of the recordings

Figure 23. Left, cavernous opening where a pressure transducer was staked with the purpose of detecting water runoff into the cave. Right, rain gauge installed on borehole marker from potash investigations in Section 3.2.

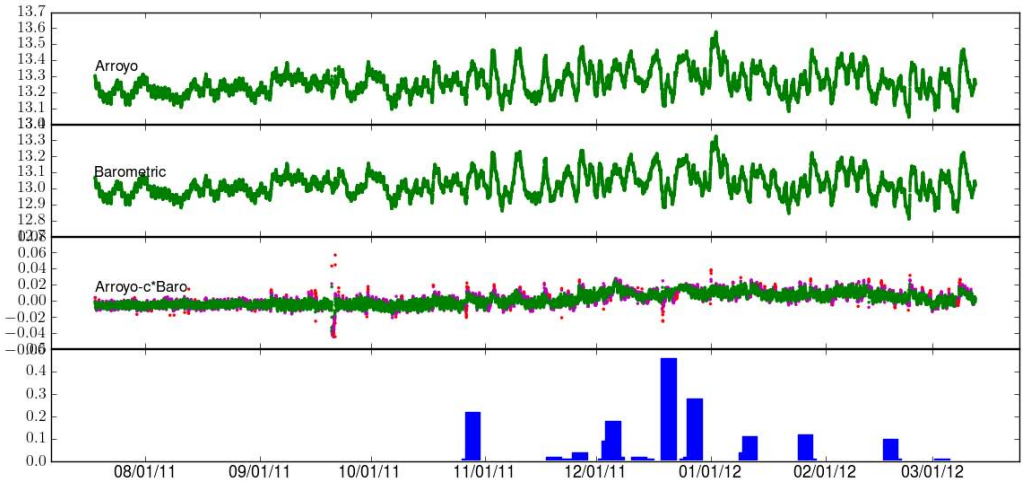

Figure 24. Results from pressure and rain experiment. Top shows the plot of the pressure gauge (given in psi) placed in the arroyo. Regional recorded barometric pressure (also given in psi) directly below. The difference between these two is given in the third row. There is nominal difference between the two, despite significant rain events (given in inches) shown in the final row.

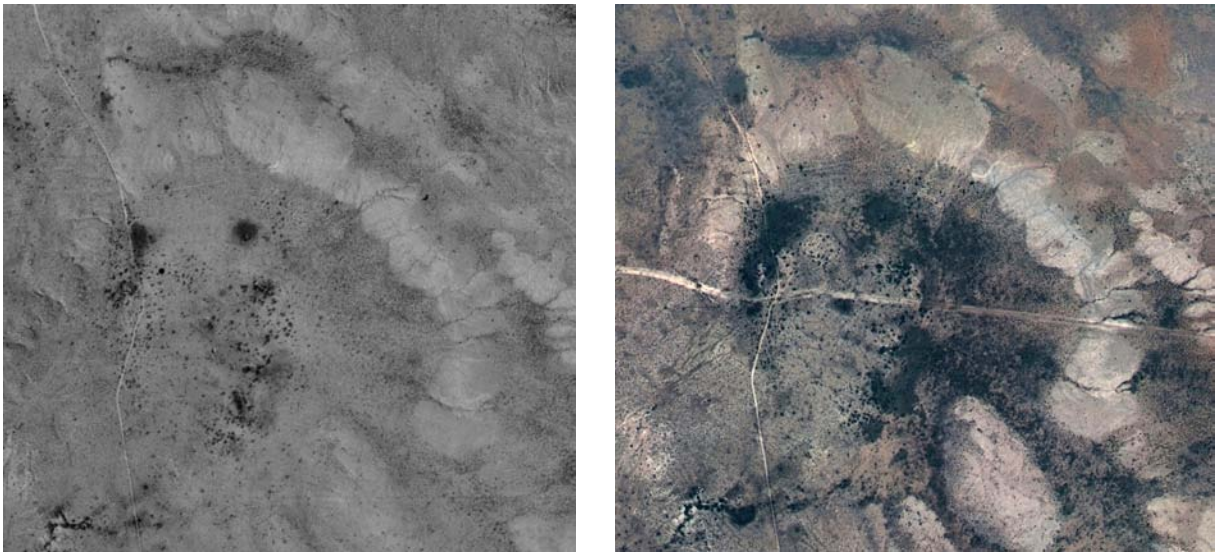

Figure 25. Aerial photographs from 1996 and 2006, left to right, shown side-by-side to illustrate the dramatic difference in vegetation dependent upon seasonal rainfall.

may qualitatively indicate the occurrence, volume, and direction of water flow. This method would also be unobtrusive and inexpensive, except for analysis labor costs.

4 Conclusion

The national, economic and energy security of the US is reliant on locating and characterizing suitable locations for energy production and waste disposal. Karst is a common geological feature; in many places, pollutants from municipal and agricultural waste have reached crucial water supplies via karst. Improved semi-arid karst characterization methodologies is crucial to the security of water systems. This research compares several geophysical techniques for achieving this goal. Since geophysical techniques can provide somewhat subjective results when performed independently, comparing multiple techniques at one location is of scientific value.

Due to the realization of technical risks, specifically the durability and applicability of WSN hardware to harsh environmental conditions, we augmented the project goals to explorer the feasibility of conventional geophysical techniques to characterizing shallow semi-arid karst features. The challenges adapting the WSN hardware to the environment elucidated several R&D tasks for future research. For example, it is recommended that super capacitors are investigated instead of lithium-ion or other common battery types. We also recommend developing simple interfaces for users to command network data collection – this is a complex task for which new algorithms might be developed to automatically optimize certain parameters.

While troubleshooting WSN challenges, we diverted resources to conduct gravity, seismic, and resistivity surveys on an area with known shallow karst. The surveys were designed over small areas to enhance data resolution – a common issue with karst characterization. Additionally, we independently constructed a conceptual geological model for comparisons. Each geophysical technique offers its own advantages and disadvantages. Our results suggest that the micro-gravity technique offers a good cost/benefit ratio for locating general karst features. However, little confidence can be achieved using only one method; a strong conceptual geological model plus two geophysical surveys is desirable. The cost of performing multiple surveys and ensuing data analysis is often cost-prohibitive. Therefore, there is still value is pursuing time-lapse resistivity (or other methods) which may avoid multiple techniques by providing stronger information through change detection, as originally hypothesized. Future research may focus on overcoming power and environmental difficulties associated with in-situ geophysical deployments. Further analysis techniques might also be developed for characterizing semi-arid karstic terrain, as very few currently exist.

This research brings to light the importance and challenges with characterizing semi-arid karst through a multi-method geophysical study. As there have been very few studies with this emphasis, this study has expanded the body of practical experience needed to protect the nations water and energy security interests.

References

[1] George O. Bachman. Geology of nash draw, eddy county, nm. Technical report, U.S. Geological Survey Open-file Report 81-31, 1981.

[2] George O. Bachman. Stratigraphy and dissolution of the rustler formation. Technical Report SAND86-7077C, Sandia National Laboratories, 1986.

[3] Dennis W. Powers, Richard L. Beauheim, Robert M. Holt, and David L. Hughes. Evaporite karst features and processes at nash draw, eddy county, new mexico. In *New Mexico Geological Society Guidebook, 57th Field Conference, Caves and Karst of Southeastern New Mexico*, pages 253–266. 2006.

[4] F. Sumanovac and M. Weisser. Evaluation of resistivity and seismic methods for hydrogeological mapping in karst terrains. *Journal of Applied Geophysics*, 47:13–28, 2001.

[5] S. Truss, M. Grasmueck, S. Vega, and D. Viggiano. Imaging rainfall drainage within the miami oolitic limestone using high-resolution time-laps ground-penetrating radar. *Water Resources Research*, 43, 2007.

[6] James D. Vine. Surface geology of the nash draw quandrangle, eddy county, new mexico. Technical report, Geological Survey Bulletin 1141-B, 1963.

[7] J. Vouillamoz, A. Legchenko, Y. Albouy, M. Bakalowicz, J. Baltassat, and W. Al-Fares. Localization of saturated karst aquifer with magnetic resonance sounding and resistivity imagery. *Ground Water*, 41(5):578–586, 2003.

A Additional 2D Gravity Results

Below are the remaining gravity data and results, included for completeness. Figure A.1 shows the NE to SW line measurements, the NNW to SSW line already given in Figure 9. There is somewhat larger variability in the corrected data in this line as opposed to the other. The last 16 points are of particular interest, these are the southernmost points in the NE to SW line. The first five of these cross over a buried oil pipeline where the first one to two meters of Magenta and alluvium were disturbed. The last 11 points shifted and sloped differently than expected – so much so, that we re-measured these points in the field on the next day under the assumption that the gravimeter was misbehaving due to heat or wind. The new measurements were similar to the first set, leaving an unexplained shifted set of data which does not display the same linear trend as the rest of the points.

Figure A.2 contains the gravity measurements for the Arroyo grid, easternmost grid in Figure 8, while Figure A.3 contains those of the GE grid, the westernmost grid in Figure 8. Neither figure gives a useful trend line, since the measurements were taken to weave back and forth across the respective grid, a better depiction is given in Figure 10. However, these do show a similar correlation to elevation as with the line data, even with data points taken near the edges of sinkholes. The remaining anomalies are also similar in magnitude to those found with the simple line data.

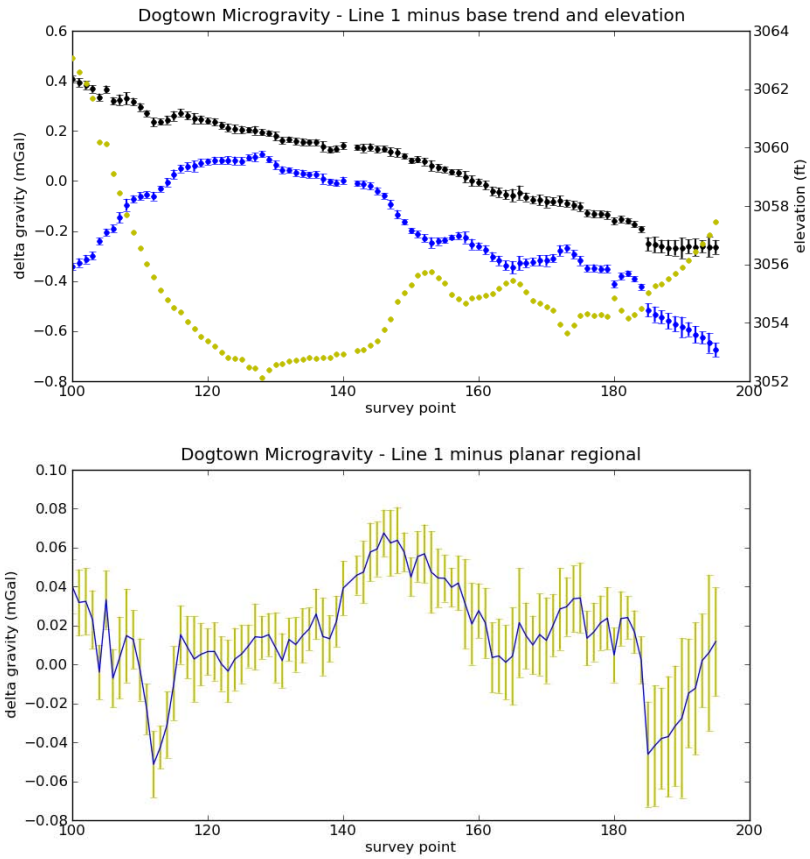

Figure A.1. Top, gravity data (minus baseline b-spline trend) in blue. Elevation is shown in yellow. The black data is the gravity data with the elevation trend removed. Below, a linear trend is removed from the data which leaves anomalies. Two standard deviations are used on either side of the mean data point to construct the error bars in both figures.

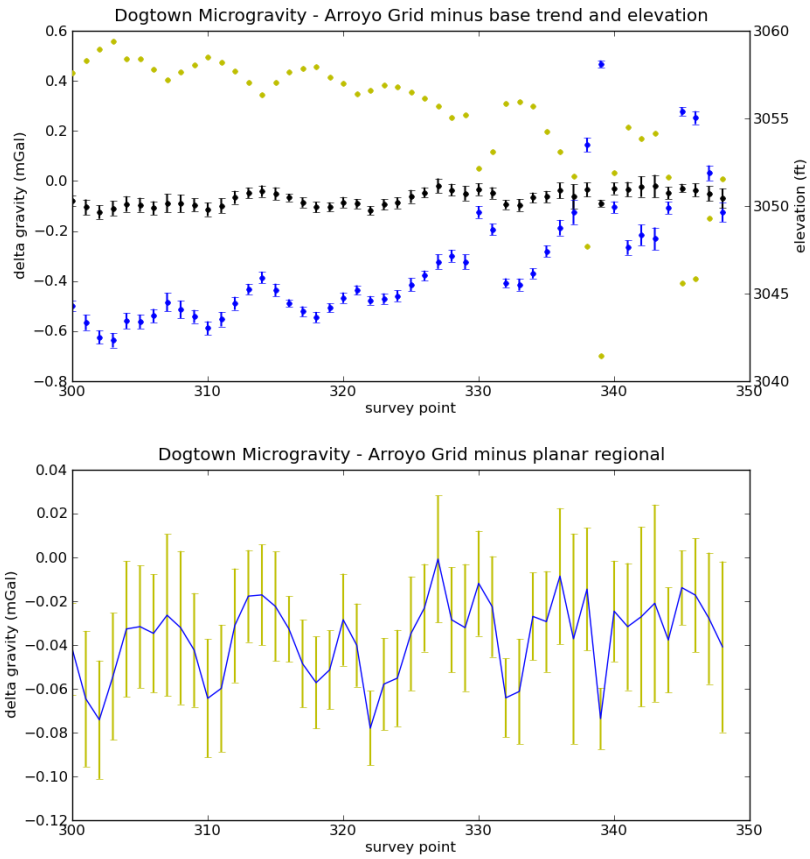

Figure A.2. Top, gravity data (minus baseline b-spline trend) in blue. Elevation is shown in yellow. The black data is the gravity data with the elevation trend removed. Below, a linear trend is removed from the data which leaves anomalies. Two standard deviations are used on either side of the mean data point to construct the error bars in both figures.

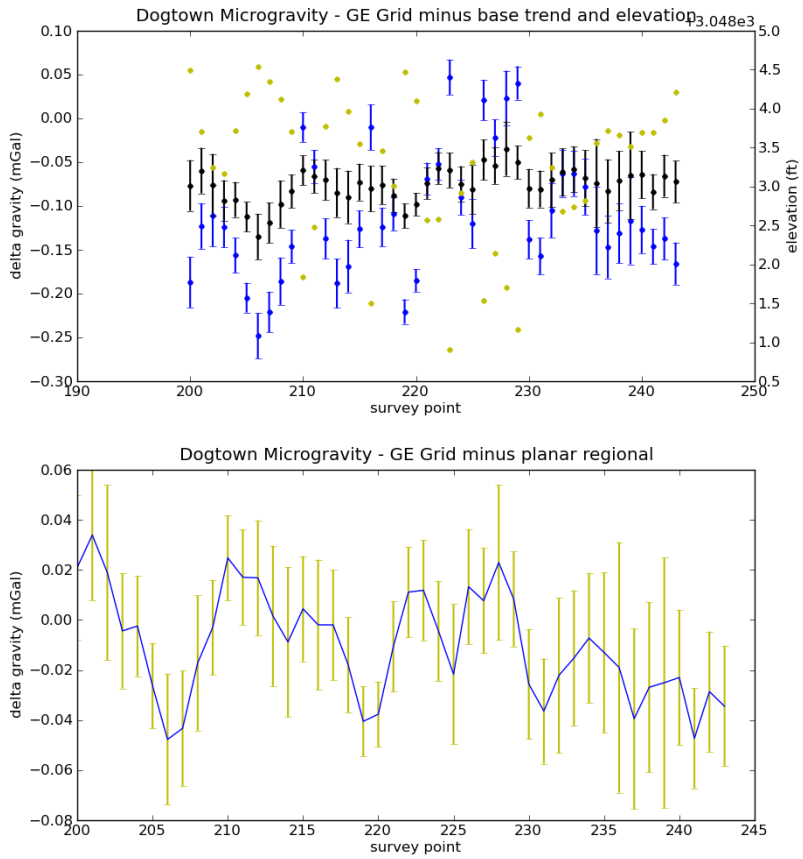

Figure A.3. Top, gravity data (minus baseline b-spline trend) in blue. Elevation is shown in yellow. The black data is the gravity data with the elevation trend removed. Below, a linear trend is removed from the data which leaves anomalies. Two standard deviations are used on either side of the mean data point to construct the error bars in both figures.

DISTRIBUTION:

1	MS 0899	Technical Library, 9536 (electronic copy)

Sandia National Laboratories